# STICS crop model and Sentinel-2 images for monitoring rice growth and yield in the Camargue region

Dominique Courault, Laure Hossard, Valérie Demarez, Hélène Dechatre, Kamran Irfan, Nicolas Baghdadi, Fabrice Flamain, Françoise Ruget

Agronomy for Sustainable Development (2021) 41: 49
https://doi.org/10.1007/s13593-021-00697-w

RESEARCH ARTICLE

# STICS crop model and Sentinel-2 images for monitoring rice growth and yield in the Camargue region

Dominique Courault[1] · Laure Hossard[2] · Valérie Demarez[3] · Hélène Dechatre[1] · Kamran Irfan[1] · Nicolas Baghdadi[4] · Fabrice Flamain[1] · Françoise Ruget[1]

Accepted: 16 April 2021 / Published online: 6 July 2021


## Abstract

The assessment of rice yield at territory level is important for strategic economic decisions. Assessing spatial and temporal yield variability at regional scale is difficult because of the numerous factors involved, including agricultural practices, phenological calendars, and environmental contexts. New remote sensing data acquired at decametric resolution (Sentinel missions) can provide information on this spatial variability. The study objective was thus to evaluate the potential of Sentinel-2 images for monitoring rice cropping systems and yield from farm to region scales. The approach considered both observations and modeling. In-depth farmers surveys were carried out in the Camargue region, Southeastern France. The novelty was to use operational tools (BVNET and PHENOTB) to compute leaf area index, to daily interpolate this biophysical variable from 44 images acquired in 2016 and 2017 for each rice field, and to derive key phenological parameters from the analysis of the temporal profiles. The STICS crop model was spatially used, considering the biophysical variables derived from remote sensing. We tested four simulation strategies, differing in the integration intensity of remote sensing information into the model. Results have shown that (1) Sentinel-2 data allowed distinguishing early and late rice varieties. (2) The phenological stages mapped at the regional level allowed to better understand the agricultural practices of farmers. (3) The assimilation of remote sensing data to the STICS crop model significantly improved yield estimation and provided useful information on the spatial variability observed at regional scale. It was the first time that Sentinel-2 data are used with STICS crop model to assess rice yield at both farm and regional scale in the Camargue area. The proposed method is based on free open data and free access model, easily reproducible in other environmental contexts.

**Keywords** Paddy · LAI · Production mapping · Remote sensing · Farm scale

## 1 Introduction

Although rice is not a staple food in Europe, this crop plays an important sociocultural (Picazo-Tadeo et al. 2009) and ecological (Longoni 2010) role in several Mediterranean countries. Timely and accurate estimations of the area of rice production and the associated yields can provide invaluable information for governments, planners, and decision-makers that need to formulate agricultural and environmental policies (Mosleh et al. 2015). Climatic and soil conditions that influence the various yield components can be reinforced or mitigated through appropriate choice of variety and technical practices such as sowing dates and fertilization (Delmotte et al. 2011). Sometimes even small changes in the sowing date, depending on climatic hazards, variety, and soil type, can lead to important yield reductions from cold-induced sterility (Confalonieri et al. 2009b). Technical practices can be used to avoid problems like weed competition (Delmotte et al. 2011). However, assessing the spatial variability of these agricultural practices through field surveys at regional scale is generally difficult, time-consuming, and costly.

An alternative is to use models for the assessment of yields. Crop models have been used extensively to analyze different practices such as applying nutrients, managing water, or

✉ Dominique Courault
dominique.courault@inrae.fr

[1] UMR 1114 EMMAH, INRAE-Avignon université, Domaine St Paul, Agroparc, 84914 Avignon, France

[2] UMR 951 Innovation, Univ Montpellier, INRAE, 2 place Pierre Viala, 34 060 Montpellier, France

[3] CESBIO-UMR 5126, 18 avenue Edouard Belin, 31401 Toulouse, France

[4] UMR Tétis, IRSTEA INRAE, Univ Montpellier, 34090 Montpellier, France

altering genetic coefficients (Boote et al. 1996; Van Keulen and Asseng 2019). Some authors such as Jin et al. (2018) reviewed the development of the crop models over time. Bregaglio et al. (2017) analyzed the potential effects of climatic changes on rice productions using two crop models and showed that advancing the sowing date and adopting varieties with longer crop cycle can moderate the impact of higher temperatures on rice yields. Li et al. (2015) point out the uncertainties in predicting rice yield by current crop models under a wide range of climatic conditions. With these issues in mind, they considered thirteen models in their study, among them, the STICS crop model (Brisson et al. 2003), whose results corresponded well with the observations (Li et al. 2015).

There are different crop model categories. Their classification can be done according to the simulated processes. Some of the most widely used rice models are ORYZA2000 (Bouman and van Laar 2006), APSIM-RICE (Gaydon et al. 2012), CERES-RICE (Singh et al. 1993), DNDC-Rice (Fumoto et al. 2008), GEMRICE (Yoshida and Horie 2010), McWLA (Tao and Zhang 2013), RiceGrow (Tang et al. 2009), WOFOST (Zhou et al. 2019), WARM (this last one being mainly applied in Italy (Confalonieri et al. 2009a)), and STICS (with a specific rice module developed by Irfan (2013)). Most models require genotype data, soil characteristics, cultivation practices, and meteorological information as forcing variables.

STICS is a generic crop model (Brisson et al. 2003) with specific modules to account for the water, nitrogen, and carbon balances in the system from the initial to final stages and the remaining quantities after the cropping season (Ruget et al. 2016). This model has proven to be robust, able to simulate a large range of pedoclimatic conditions, and behave well in the intercomparison of rice crop models through the AGMIP program (Li et al. 2015). It has been calibrated from a large dataset and is well suited for the Camargue area (Irfan 2013; Bregaglio et al. 2017).

While the implementation of STICS is relatively easy at the local scale where the main characteristics of the soil and agricultural practices can be gathered from punctual measurements or from surveys, its application at a larger scale is more difficult because soil, climate, and crop management can vary considerably. A lack of knowledge about spatial variations in these factors leads to uncertainties, mainly affecting physiological growth simulations that can induce large errors in yield estimations (Jin et al. 2018). Hansen and Jones (2000) have reviewed different approaches in applying crop models at scales larger than individual fields. They conclude that the most rigorous approach requires characterizing the spatial distribution of all model inputs, but this can be very difficult due to the complexity of the model considered. The requested parameters can indeed be very numerous and almost impossible to inform, unless expensive and time-consuming field campaigns are conducted. Some approaches have proposed to use statistical methods, but these approaches sometimes involve significant assumptions based on distributions and related probabilities (Hansen and Jones 2000). Paltasingh and Goyari (2018) proposed a review on the statistical modeling of crop-weather relationship in India. Shi et al. (2013) compared three main statistical methods using historical data and identified the main issues related to the extent of spatial and temporal scale, non-climatic trend removal, collinearity existing in climate variables, and non-consideration of adaptations.

Other approaches have used remote sensing, where continuous and temporal information can be provided from a wide range of sensors operating all over the world (Courault et al. 2016). Remote sensing data have often been combined with crop models to improve their performance for yield prediction, mostly for cereals (Battude et al. 2017) or beets (Launay and Guerif 2005). Jin et al. (2018) and Delecolle et al. (1992) describe various assimilation methods. The choice of method depends on various factors, such as model complexity, computing time, and the number of parameters to estimate.

Forcing methods generally involve biophysical variables such as LAI (leaf area index) as input data in crop models (Clevers et al. 2002; Courault et al. 2010; Tripathy et al. 2013; Yao et al. 2015). Inversion methods are commonly used for model calibration with, for example, the simplex search algorithm (Battude et al., 2016; Claverie et al. 2012). More complex variational or sequential approaches (which require more computing time) are also found in the literature (Jin et al. 2018). A review on the practical aspects of data assimilation is presented in Jarlan and Boulet (2014).

Microwave remote sensing has the advantage of acquiring images in any type of weather and has often been used in tropical areas for rice yield assessment (Bouvet and Thuy Le 2011; Bouvet et al. 2014; Pazhanivelan et al. 2019; Shen et al. 2009). Sentinel-1 images have shown a high accuracy to identify rice fields (Bazzi et al. 2019). Chakraborty et al. (2005) have used RADARSAT data to estimate crop height, among other rice crop parameters.

In Mediterranean regions, as the weather was less cloudy than tropical regions, many studies have preferred to use optical data in crop models (Courault et al. 2010; Tornos et al. 2015; Gilardelli et al. 2019). Biophysical variables derived from optical data such as LAI developed from operational algorithms like the BVNET tool (Baret et al. 2007) have proven their robustness and are widely used. Such products (LAI) are now freely distributed through different remote sensing platforms (e.g., https://lpdaac.usgs.gov/products, and https://www.theia-land.fr/en/products/). Operational vegetation indexes, such as MODIS-derived EVI, have also been used for yield estimations at large scale (Palakuru and Yarrakula 2019; Zhou et al. 2019). Other MODIS products (MOD9, MOD13) have been analyzed in different pedoclimatic contexts (Boschetti et al. 2015; Manfron et al. 2012). However,

the spatial resolution of MODIS products (1 km) does not allow to distinguish different management practices at the scale of a single farm (Merlin et al. 2010). Downscaling methods have been proposed, combining low- and high-resolution data to gain a deeper understanding of crop system dynamics, but the developed methods are not currently used routinely for operational applications (Gilardelli et al. 2019).

Until recent years, the issue of temporal and spatial resolution of most remote sensors posed the greatest challenge. Data from low spatial resolution imagery were not suitable for distinguishing practices at the field scale. This issue was resolved from June 2015, the launch of the first Sentinel-2A satellite which provides a large and unprecedented amount of free data with high-resolution images (10 m, every 10 days in 2016 and every 5 or 3 days since the Sentinel-2B launch in March 2017). These data are particularly well suited for crop monitoring in Mediterranean regions where the days are often dry and clear.

The objectives of our study were then to evaluate the contribution of Sentinel-2 dataset in two undertakings: (1) to monitor the phenological calendar of rice plots in order to better understand the agricultural practices of the farmers and (2) to assess rice production and its spatial variability at regional scale for the whole Camargue, combining the STICS crop model and remote sensing data. The developed approach also aims to propose an operational method to get annual map of rice production for various territory stakeholders.

## 2 Materials and methods

### 2.1 Study area and rice crop management

The Camargue area in southeastern France (center 43° 36′ 4.31 N–4° 33′ 23.22 E, 5 m above sea level on average) is a large wetland plain of 145,000 ha located in the Rhone delta. Approximately 70,000 ha is used for agricultural production, and the remaining land is a nature reserve (UNESCO reserve since 1977). The region is characterized by warm summers (with average daily temperatures varying between 18.5 and 27°C over the period 1991–2020) and mild winters (daily minimum temperatures are usually higher than 0°C and can reach up to 17°C in some years). Precipitation mainly occurs in the autumn and winter months (603 mm for annual average from 1991 to 2020), with large interannual variations. The Fourques station (43.704 N 4.561 E) recorded 564 mm in 2016, but only 277 mm in 2017 (Supplementary Material 1). Strong and prevalent winds (known as *le Mistral*) cause significant evapotranspiration of up to 1300 mm/year. The high water deficit promotes the capillary rise of saline ground water (Trolard et al. 2018). Flooding of rice fields from March to September contributes to the desalinization of the soil (irrigation from the Rhone river provides roughly 25,000 to 30,000 $m^3 \cdot ha^{-1}$ of water each year). The main soil types correlate with small variations in the topography. There are hydromorphic shallow soils and deeper soils with a higher sand content. Four soil types have been defined at the regional scale (Ruget et al. 2016): sandy soils and clay soils, each classified as deep or shallow (topography above or below 1.5 m.a.s.l., corresponding to salinity pressure).

Rice farming constitutes the most widespread crop in the delta, either in rotation with wheat or as a monoculture. The rice cycle lasts between 80 and 120 days depending on the variety and the weather conditions. Cultivated rice belongs to the *Oryza japonica* ecotype, which adapts well to large variations in climate, from tropical to Mediterranean. Water management is crucial all along the growth cycle, from sowing to harvest. Small channels are dug in bare fields to better regulate irrigation and drainage (see Fig. 1a). Most farmers sow 4 to 5 days after flooding. The minimum temperature for emergence is 12°C and for flowering 20°C. Depending on the choice of cultivar (early or late), the soil type (shallow and deep), and the temperature, sowing dates can extend from mid-April (DOY 105) to the end of May (DOY 148). Management of the water level and the water temperature are also essential factors for seedling emergence and weed control. Successive depletion and replenishment results in variations of 15 to 30 cm in the water level, which is regulated according to the climate and crop interventions. For example, farmers lower the water level during weeding operations and try after to keep a certain level of water for thermal regulation. During the growing period, nitrogen fertilizer can be applied 2 to 3 times (total of 150 $kgN \cdot ha^{-1}$ in average). Harvest usually starts in mid-September (DOY 258) and continues until the end of October (DOY 288). The grain humidity must be below 22% for the rice to be harvested.

Stubble management varies between farms. Some farmers bury the stubbles and plow the soil immediately in order to sow a new crop. Others prefer to burn rice straw residues (Fig. 1f), even though this practice is increasingly seen as problematical because of the negative impact on the environment (Delmotte et al. 2011). During winter, some rice fields are left fallow or planted with alfalfa to increase soil nitrogen content.

### 2.2 Ground observations and surveys

During Sentinel-2 acquisitions in 2016 and 2017, ground observations of 830 fields were made for land use identification throughout the Camargue area. In 2017, hemispherical photographs were taken over 12 rice fields at the same dates than Sentinel-2 along the crop cycle, in accordance with the Valeri protocol (http://w3.avignon.inra.fr/valeri/). These photographs were then processed by Can-eye software (https://www6.paca.inra.fr/can-eye) to estimate the LAI to monitor crop growth.

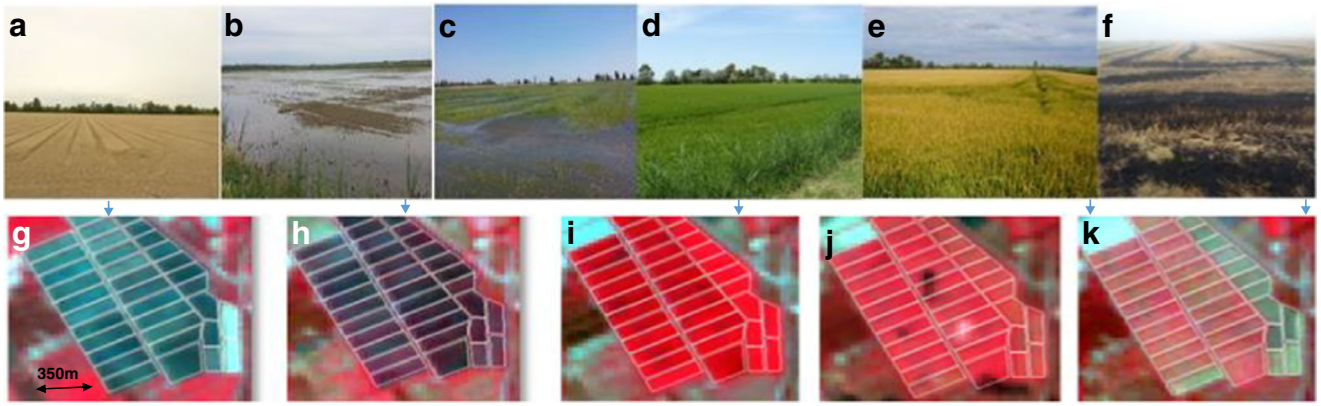


**Fig. 1** Top photos show the different surface states of rice fields: **a** soil preparation, plowing with small channels for irrigation, **b** flooding, **c** crop emergence, **d** maturity stages, **e** senescence before the harvest, and **f** residues burned in October. Lower photos (**g** through **k**) show colored compositions of Sentinel-2 images over rice fields during the growing cycle. Coded in red, band 8 (near-infrared range); in green, band 4 (red); in blue, band 3 (green); the images are taken from April to October 2016 at the main stages of rice development displayed above.

Additionally, seven farms with crop surfaces varying from 170 to 490 ha, including more than 200 rice fields, were surveyed about a number of specific agricultural practices and elements: soil preparation, sowing date, rice variety, plant density, water management, chemical treatments, fertilizer dates and quantity, harvest date, production, and residue management. The average size of rice fields was around 3 ha. In 2016, 298 fields were cultivated in rice on these farms; in 2017, they cultivated 243 rice fields. These farms were chosen as representative of the soil and variability of practices encountered throughout the Camargue region. In each farm, we observed a variability of crops and practices (e.g., rice cultivars, sowing dates; see Supplementary Material 2).

## 2.3 Sentinel-2 data

In 2016 and 2017, 44 cloud-free Sentinel-2 images (24 in 2016, 20 in 2017, acquired from DOY 100 to DOY 290) were downloaded from the THEIA platform (http://www.theia-land.fr/) at level 2 (georeferenced in UTM projection and corrected from atmospheric effects according to the MAJA chain described in http://www.cesbio.ups-tlse.fr/multitemp/).

The first stage was to separate rice from the other crops. A land use map was made using the following spectral Sentinel bands, B3 green, B4 red, B8 near-infrared, and B12 middle infrared band, and 6 dates were chosen from April to October to separate at the best the various crops. A supervised non-parametric classification algorithm, support vector machine (SVM), has been used considering the ground observation points mentioned above. SVM is basically a binary classifier that delineates two classes by fitting an optimal separating hyperplane to the training data in the multidimensional feature space to maximize the margin between them (Ndikumana et al. 2018b). Among the 830 ground observations, 400 were used for the learning step and 430 for the validation. We defined 4 classes: rice, wheat, grassland (the dominant crops) and the last class which groups all other crops. The learning dataset was chosen in order to include the main crops encountered in the study area; the rice surfaces covered 800 ha in the learning dataset and 900 ha in the validation dataset. The fields were selected from a wide spatial distribution in order to cover the spatial variability of practices and soils. Accuracy was evaluated by computing the confusion matrix and the kappa index.

The second stage consisted in computing the biophysical variable (LAI) at each date to get information on the phenological calendar of each rice field. LAI were estimated using the BVNET tool and the Sentinel-2 reflectances of the three spectral bands B3, B4, and B8. BVNET relies on reflectance simulations made from the PROSAIL radiative transfer model combined with a neural network (Baret et al. 2007). The solar and sensor angles are necessary for computation. The normalized difference vegetation index (NDVI) was also computed for each image to extract the sowing date according to the method described in Courault et al. (2020) (a brief summary is given in Supplementary Material part 3).

In order to obtain the boundaries of each field in the Camargue area, we used Envi software to build a shapefile based on the land use map obtained for each year studied (vectorization of the initial raster format). To compensate for limits in the accuracy of our pixel scale classification (vectorization did not always match actual field boundaries), we merged, using QGIS3.6.3 software, the boundary information obtained from the RPG file (IGN http://professionnels.ign.fr/rpg) corresponding to the fields as declared by farmers requesting subsidies. To avoid edge effect, we allowed for a buffering of 3 m between the fields, and to complete the file, all of our ground observations were also considered. The resulting shapefile was then overlaid with all the raster LAI and NDVI images for each Sentinel-2 date in order to extract the mean and standard values for each rice field. This step was done using QGIS3.6.3 software and zonal stats functions

developed with R software. Finally, excel files containing the mean value of LAI and NDVI for each field (3453 and 3645 rice fields in 2016 and 2017, respectively) and for each date were analyzed according to information collected with farmers.

Figure 2 details the different steps of image processing up to crop modeling. The models and software are in gray boxes. The boxes in red underneath summarize the key points. The next step consisted of fitting a phenological model (double logistic function, see Eq. 1 in Supplementary Material part 4) to the LAI observations. We used the algorithm proposed by Inglada (CESBIO Toulouse, http://tully.ups-tlse.fr/jordi/phenotb). The parameters were optimized using a Levenberg-Marquardt optimizer available in the free OTB toolbox. Key phenological parameters such as the emergence and senescence dates and the length of maximum development were derived from the temporal profiles (see Supplementary Material part 4).

## 2.4 Description of the STICS crop model

STICS is a generic crop model (Brisson et al. 2003) adapted for rice by Irfan (2013) and Ruget et al. (2016), which simulates crop phenological development at a daily time-step as a function of thermal time accumulation. The model's structure is modular, with each module representing a process: development, conversion, grain formation, water balance, transformation of assimilates into grain, and water and nitrogen cycles. The model can consider different farming management practices as inputs.

Leaf growth was simulated based on development rates, development stages, temperature, and water and nitrogen stresses (see Supplementary Material 5). Possible water and nitrogen stresses are assessed with three indices that can reduce leaf growth and biomass accumulation. They are calculated from the water and nitrogen balances. For our study case, we did not consider the limiting effects of water because rice cropping systems are flooded all along the cycle. To maintain the flood conditions from the sowing date to the beginning of September, approximately 25 irrigations were undertaken, varying from 20 to 40 mm every 5 days (the total water amount varies from 500 to 800 mm depending on weather conditions).

The simulated LAI is used to estimate photosynthesis and respiration and then to compute the biomass. The biomass was transferred into yield using a harvest index, which is upper limited by the product of grain number by maximum grain weight. The maximum value of radiation use efficiency is modulated by temperature, radiation, and crop development stage (see Supplementary Material 5 for more details).

STICS requires daily weather inputs (Table 1) and soil descriptions of the corresponding layers characterized by their chemical and physical properties (for the rice, two soil layers were defined, a first layer of 25 cm and a second thin soil layer of 5 cm with a low value of infiltration at 0.01 mm/day to obtain an impermeable soil layer to avoid water loss). Four soil types were defined in the Camargue region by Ruget et al. (2016), distinguished mainly by their clay and organic nitrogen contents (see Table 2 in Supplementary Material 5).

The main parameters used for our simulation are reported in Supplementary Material 5, Table 1. Since most encountered

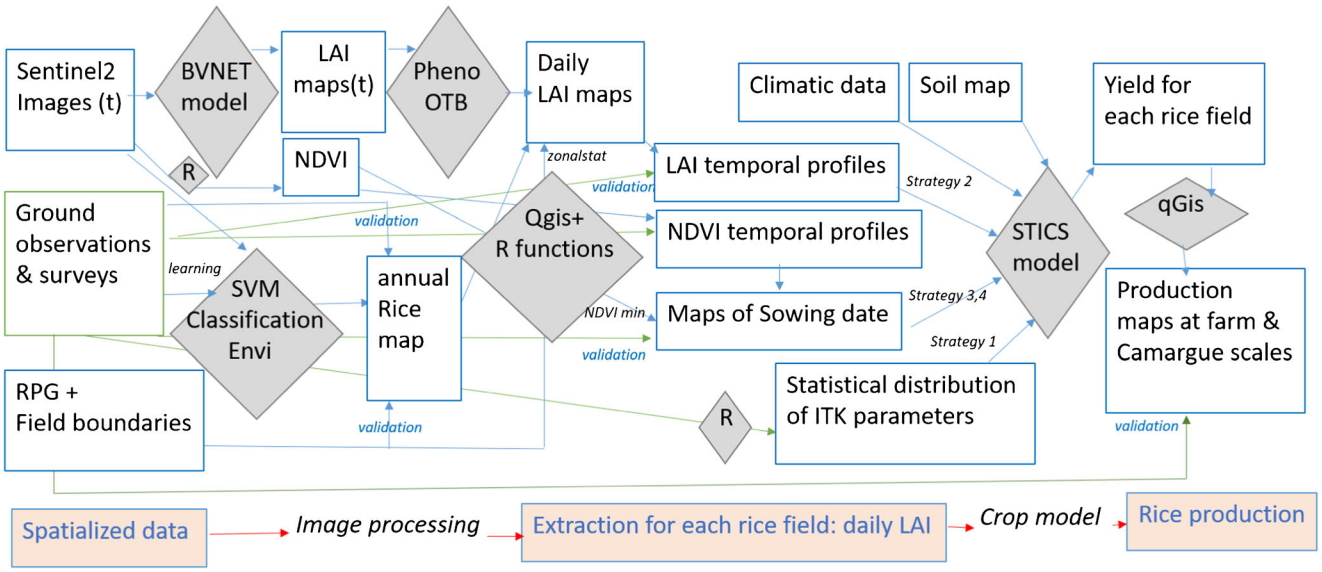


**Fig. 2** Scheme summarizing the main steps of image processing up to crop modeling. Sentinel-2 data are acquired at different dates (*t*). The land use map is obtained from a supervised classification (SVM support vector algorithm); the shapefile contains all the field boundaries (built from the land use vectorization merged with the RPG (Registre Parcellaire Graphique) file); ITK parameters mean all parameters describing the main agricultural practices; LAI, leaf area index.

**Table 1** Main inputs of STICS related to the climate, soil, plant characteristics, and technical practices and their sources for the different simulation strategies. *N* for a normal distribution, the first argument is the mean value, and the second the standard deviation, *U* for uniform distribution.

| | Main inputs | Source |
|---|---|---|
| Climate | Precipitation, air temperature, air moisture, global radiation, wind speed | Fourques station (data downloaded from the Climatik toolbox (database Agroclim INRAE AVIGNON)) |
| Soil | Tillage depth, physical and chemical properties, water holding capacity, soil nitrogen status | Soil map with 4 classes defined by Ruget 2016 (see Table 2 in Supplementary Material 5)<br>(For the strategy 4: Norg and Nmin are assessed from Sentinel-2 LAI) |
| Plant/variety | Duration of different growth stages, grain weight temperature required for growth and grain filling | For strategy 1: Semi-early variety chosen (Ariete parameters, see Table 1 in Supplementary Material 5, LAI is simulated by STICS)<br>Strategies 2-3-4: LAI from Sentinel-2 is used as input data, the other plant parameters are the same as in strategy 1 (see Table 1, Supplementary Material 5) |
| Management practices | Sowing date (*iplt0* unit DOY) | Strategy 1: *iplt0* drawn from the statistical distribution, N(130,10)<br>Strategies 2-3-4: *iplt0* estimated from Sentinel-2 (Kennedy 2018) |
| | Ammonium phosphate date (*julapN(1)* DOY) | Strategies 1-2-3-4: drawn from statistical distribution, N(111,4) and N(167,7) |
| | Urea date before sowing (*julapN(2)* in DOY) | Strategies 1-2-3-4: julapN(2)+ N(68,10) |
| | Urea date after sowing (*julapN(2)* in DOY) | Strategies 1-2-3-4: julapN(2)+N[24;34] |
| | Ammonium phosphate dose (*doseN(1)* kgN·ha$^{-1}$) | Strategies 1-2-3-4: drawn from statistical distribution, N(54,12) |
| | Urea dose (1 or 2 intake) (*doseN(2)* kgN ha$^{-1}$) | Strategies 1-2-3-4: drawn from statistical distribution, N(52,12)/N(106,8) |
| | Organic nitrogen in the soil (*Norg*, %) | Strategies 1-2-3: 0,15; strategy 4 simplex optimization U[0,10;0,25] |
| | Mineral nitrogen in the soil ($NO3_{init}$, %) | Strategies 1-2-3: 32; strategy 4 simplex optimization U[0;30] |

rice varieties in 2016 and 2017 were semi-early, we chose to use the parameters defined for the Ariete variety for all simulations (see values given for the main processes in Supplementary Material part 5, based on Bregaglio et al. 2017).

The agricultural practices for each field (sowing date, fertilizer dates, and quantities) were identified through our surveys with the farmers. The surveys showed a large variability in nitrogen inputs (N); thus, nitrogen stress was activated in our simulations. Four simulation strategies were evaluated (described in the next section).

## 2.5 Studied cases

The analysis of all surveys showed a large variability in the agricultural practices. Most farmers use conventional management with herbicides and nitrogen fertilizer to promote tillering. Nitrogen is generally applied on two dates, the first with ammonium phosphate or urea at a dose of 52 kgN·ha$^{-1}$ on average (end of April) and the second averaging 106 kgN·ha$^{-1}$ (end of June). A bimodal distribution was fitted by a normal law on these collected values and analyzed using the R function fitdist, of the R package fitdistrplus (Delignette-

**Table 2** Results of the different simulations made with STICS according to the strategies described in Section 2.5 for 2016; $R^2$ determination coefficient between yield observed and simulated (t·ha$^{-1}$), *RMSE*, root mean square error; bias average difference between simulation and average yields; interval [min ; max]. *P* *P*-value, *C* Camargue level (156 fields), *F* farm scale (50 fields).

| No strategy | Initial parameters and variables | $R^2$ | *P* | *RMSE* (t·ha$^{-1}$) | Bias (t·ha$^{-1}$) | Interval (t·ha$^{-1}$) |
|---|---|---|---|---|---|---|
| 0 | Constant values | - | - | 0.64 | +0.64 | 5.74 |
| 1 | Randomly drawn from statistical distributions | C:0.13<br>F:0.04 | 0.26<br>0.79 | 2.90<br>4.70 | 3.70<br>4.70 | C:[4.01–9.10]<br>F:[7.90–9.00] |
| 2 | Daily LAI Sentinel-2 + parameters drawn from the distributions | C:0.56<br>F:0.24 | <0.01<br>0.13 | 1.29<br>1.26 | −0.05<br>1.00 | C:[3.10–5.90]<br>F:[3.10–5.71] |
| 3 | Daily LAI + sowing date Sentinel-2 + other parameters drawn from distribution | C:0.34<br>F:0.53 | <0.01<br><0.01 | 1.35<br>1.26 | 0.09<br>1.16 | C:[3.0–5.22]<br>F:[3.50–5.70] |
| 4 | Optimization Norg, Nmin from LAI Sentinel-2 + SD + other parameters drawn from distribution | C:0.27<br>F:0.50 | 0.02<br><0.01 | 1.59<br>0.53 | 0.80<br>0.23 | C:[3.02–5.40]<br>F:[3.50–5.22] |

Muller and Dutang 2015). This led to two normal distributions for nitrogen fertilization dates, N (111,4) and N (167, 7), and two for nitrogen amounts: N (52,6) and the second N (106,8). Farmers' practices did not significantly differ between the two years, with farmers applying fertilizers similarly from 1 year to another in response to observed crop development.

In the same way, we observed that the sowing dates were spanned several weeks, from mid-April to the beginning of June. A slight difference was observed between 2016 and 2017, with a little more variability in 2017 than in 2016. The spring of 2017 was rainy with low temperatures, particularly in April, leading the majority of farmers to sow later than usual, around the 10th of May (corresponding to a normal distribution N (130,10)). Statistical analyses (scatterplots to analyze 2 by 2 correlations) between the studied variables have shown that variables are not interdependent.

We compared different simulation strategies, in order to evaluate the use of remote sensing information into the crop model.

- Strategy 0: STICS is used without remote sensing data information, considering constant inputs. A reference field was chosen considering the most represented cultivar (Ariete) and soil (silty clay). Mean values were taken from the surveys for the agricultural practices.
- Strategy 1: Corresponded to the standard case with only the soil map as spatialized information. The fertilizer dose, application date, and sowing date are defined for each rice field from a random draw in the distribution established from surveys. A probability $P$ of 0.55 was randomly assigned to the fields receiving 2 or 3 applications of fertilizer, with the "probability of success" (the highest value) corresponding here to two applications because the data showed 55% of the parcels receiving two applications while 45% received three. LAI values are simulated by STICS (according to equation given in Supplementary Material 5), and yield estimations are compared to values provided by the surveyed farmers. No remote sensing information is used in STICS. (Remote sensing data are used in this case only to establish the rice map.) Simulations are done for each rice field for the two years.
- Strategy 2: The mean values of LAI, computed for each rice field from Sentinel-2 data and interpolated daily, are used as forcing inputs in the STICS crop model. All other parameters remain the same as in strategy 1. This study case was aimed to quantify the impact that accounting for the spatial variability of LAI has on the yield estimations.
- Strategy 3: The sowing dates (SD) are estimated from Sentinel-2 NDVI time series using a method described by Courault et al. (2019, 2020) and Kennedy (2018) (see Supplementary Material 3). SD and LAI are estimated from remote sensing data computed for each field and are introduced as forcing inputs in the crop model. The difference with the previous case was the additional information on the sowing date assumed known in the model (derived from Sentinel observations).
- Strategy 4: Sentinel-2 LAI values are used to calibrate two unknown soil parameters: initial soil organic nitrogen content (Norg) and soil mineral nitrogen content (Nmin). The simplex algorithm (Nelder and Mead 1965) is used for this optimization. Constraints are given for the maximum values (140 KgN/ha for Nmin, and 0.09 % for Norg), to have realistic values according to the expert knowledge of F. Ruget and measurements available in the area. SD is estimated from Sentinel-2 and used as input data. This case was studied because nitrogen has an important effect on rice growth and on LAI. Field experiments and farmers' perceptions consistently identify soil quality and fertilizer use as factors that can explain yield variability. There are also interactions between soil properties (percentage of clay) and nitrogen quantities (Irfan 2013). The organic nitrogen content in the soil (Norg), which is related to the field history (pre-rice, crop before rice, vegetables or alfalfa, etc.), and the mineral nitrogen content (essentially $NO_3$ brought by farmers), which is assimilated by the plant (only a residual part remains in the soil and impacts crop growth), are two key variables that are difficult to determine for the entire region. These quantities vary according to the biological activity in the soil, temperature, and oxygenation and are generally difficult to assess (Delmotte et al. 2011).

To better analyze this nitrogen impact on the main variables, preliminary sensitivity analysis has been done by varying both nitrogen inputs and soil type, with and without activating the nitrogen stress in the model. The results obtained on the simulated LAI compared with the observed LAI from Sentinel-2 are shown in Supplementary Material part 6. LAI simulations with activated nitrogen stress were closer to the observations, outlining the strong impact of nitrogen. The nitrogen also influences strongly the biomass estimation. The highest clay soils with high content of Norg present also the highest biomass. So, it appeared relevant to retrieve these initial values through assimilation method, based on remote sensing observation, as LAI was also a good indicator for crop development and easily derived from Sentinel-2 data.

Table 1 summarizes the main inputs of STICS model and their sources according to the cases studied.

The performances were evaluated at two scales: the farm and the Camargue region. Root mean square error (RMSE) and bias were computed between simulated and observed yields. Note that the yield data provided by the farmers were sometimes more or less precise and include different water contents for the grain (between 18 and 22%). A correction for water content was applied to compare only dry yield to

STICS simulations. Some farmers gave average values for the same rice variety, others clustered several fields according to their water management (small areas called *îlots*), and still others gave values for each rice field.

## 3 Results and discussion

The global accuracy of the land use map was 88% of well-classified crops (rice, wheat, and grassland) and 99% for the rice class, which was quite satisfactory. Details on the statistical scores can be found in Courault et al. (2020). Rice and wheat can be easily distinguished because their cultural cycles are staggered in time (wheat being sown in winter and harvested at the end of July and rice being sown in April and harvested in autumn). The different dates chosen for Sentinel-2 classifications allowed a good discrimination between these two main crops. It is important to mention that other methods based on the use of Sentinel-1 images can provide also good results to identify rice crops as shown by Bazzi et al. (2019) and Ndikumana et al. (2018a).

### 3.1 LAI analysis and variability of phenology parameters

Effective LAI obtained from hemispherical photographs processed with the Can-eye software (described in Section 2.2) was compared to LAI computed from BVNET. The root mean square error (RMSE) was 0.9 $m^2/m^2$ for the maximum growth period. The BVNET algorithm was also previously evaluated on Camargue rice over a longer period with similar optical data and gave 17% error with an RMSE between observed and simulated LAI of approximately 0.8 $m^2/m^2$ (Bsaibes et al. 2009).

LAI maps computed for each Sentinel-2 date (Fig. 3a) showed wide variability in rice growth at the scale of individual farms.

#### 3.1.1 Analysis at the farm scale

We selected the farm where the most detailed input data were provided by the farmer (Supplementary Material 2). We observed intra-field heterogeneities, which can be partly explained by the plant density and soil variability. In Fig. 3a, rice LAI at mid-July 2016 varied from 2 to 4 $m^2/m^2$. These differences were explained primarily by a difference in the variety (Opale ½ early cultivar and Apollo, medium cultivar sown at the same date 5/5, information given by the farm survey). In 2017 (Fig. 3b), rice fields with Opale cultivar were sown on April 27 while fields with Volando cultivar were sown later (May 16). Figure 3c shows the temporal profiles of the mean values of LAI extracted for the same Opale rice field displayed in Fig. 3a for both years, 2016 and 2017. We can clearly detect that the studied field was sown 9 days earlier in 2017 than in 2016. LAI values were higher at the maximum period in 2017 than in 2016. Rice growth was faster at the beginning of the cultural cycle in 2017 than in 2016, partly because of the difference in the sowing dates and partly because of the weather conditions (see Supplementary Material 1). Spring temperatures were higher in 2017 than they were in 2016, particularly in May (the Fourques station recorded a mean value of 17.9°C in May 2017 compared to 16.6°C in 2016). The 2017 conditions were thus very favorable for crop development, with favorable plant densities. This resulted in the higher yield observed for this field in 2017 (4.7 $t{\cdot}ha^{-1}$, value given by the farmer, field cultivated with the Opale cultivar) than in 2016 (3.5 $t{\cdot}ha^{-1}$, value given by the farmer). The crop cycle shifted in 2017 in comparison with 2016 by approximately 24 days, resulting in an earlier harvest date in 2017 (September 14) than in 2016 (October 9).

The LAI profile in 2016 also showed a small peak around the end of May, followed by a rapid decrease and then regular growth again in July. The first decrease observed corresponded weeding interventions that occurred on May 25 and June 16, 2016. In 2017, a chemical weeding treatment was applied just before sowing. Weeds and soil salinity are among the main factors affecting rice growth. A higher density of rice plants ensures greater competition with weeds and a sufficient number of panicles per unit area at harvest (Delmotte et al. 2011). The density reported in our survey varied from 207 to 344 plants/$m^2$. The simulations presented in the next section use the mean value of 310 $p{\cdot}m^{-2}$ for all strategies studied.

#### 3.1.2 Analysis for the entire Camargue area

The use of the phenological model (described in Supplementary Material 4) to obtain daily LAI values provided key parameters that allowed the monitoring of rice growth. The quality of the temporal interpolation for all fields and all dates was analyzed with classical statistical criteria, resulting in an RMSE value of 0.62 $m^2{\cdot}m^{-2}$ for 2016 and 0.58 $m^2{\cdot}m^{-2}$ for 2017, with biases of 0.17 $m^2{\cdot}m^{-2}$ and 0.09 $m^2m^{-2}$, respectively. The mean error of the LAI maximum is approximately 0.33 $m^2{\cdot}m^{-2}$. This is on the same order of magnitude of errors obtained between in situ measurements which vary from 0.1 to 0.8 $m^2{\cdot}m^{-2}$, depending on the dates (Bsaibes et al. 2009), and LAI estimations reported by Demarez (2018). LAI estimations can thus be considered satisfactory.

Figure 4 shows the statistical distributions of the main land surface phenology parameters computed for all rice fields in the Camargue area. The different parameters *t0*, *t1*, *t2*, and *t3* are computed according the method described in the Supplementary Material part 4, and for more details see *http://tully.ups-tlse.fr/jordi/phenotb*. Analysis of the emergence (*t0*), senescence (*t3*) dates, and length of the plateau (*L*) (at maximum LAI values) confirmed that rice

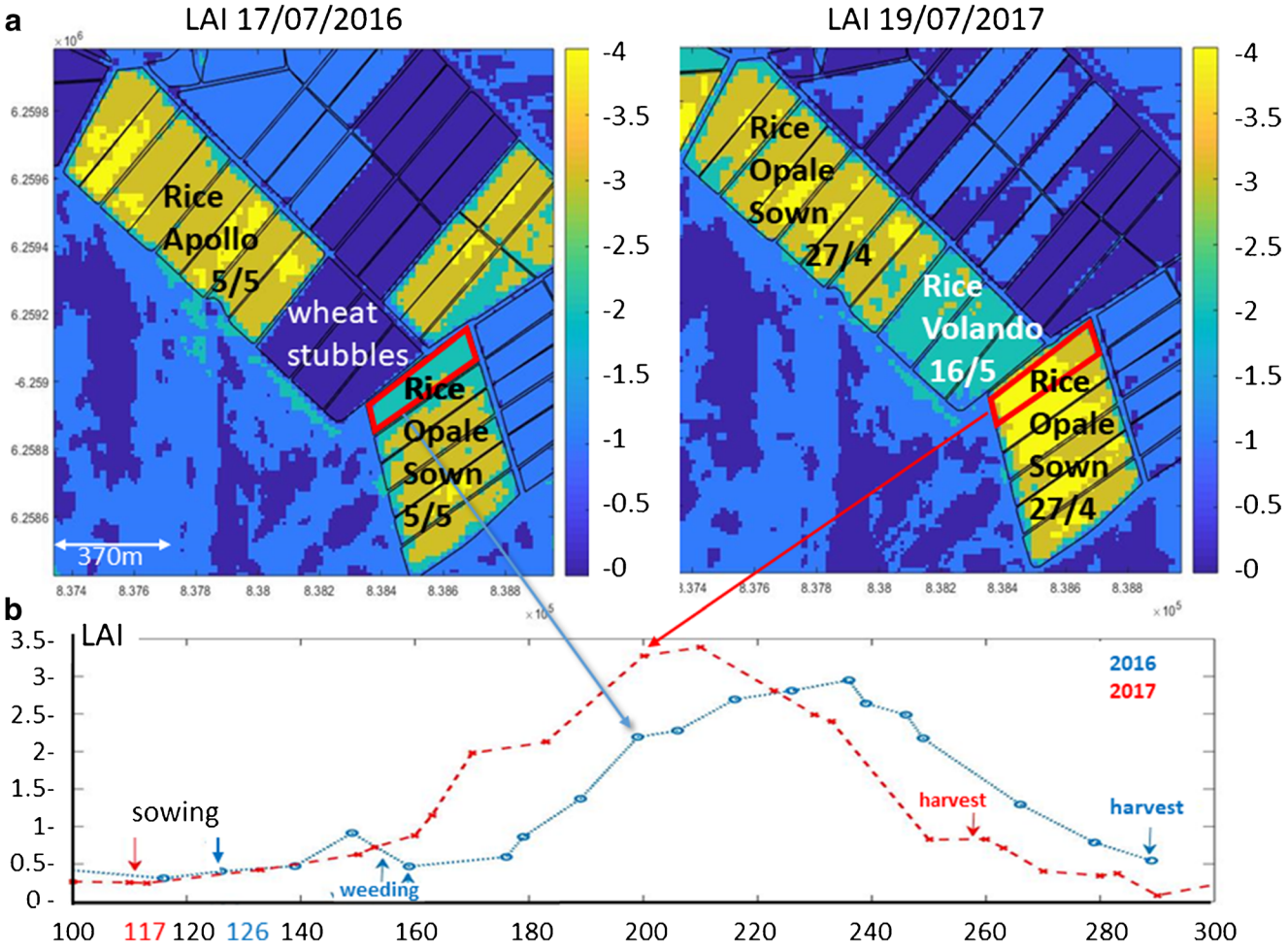


**Fig. 3** LAI (leaf area index, $m^2 \cdot m^{-2}$) maps obtained from Sentinel-2: **(a)** acquired on July 17, 2016, and **(b)** on July 19, 2017 (the x- and y-axes give the Lambert coordinates). Graph: **(c)** LAI temporal profiles obtained for the same field (Opale cultivar) for the two years studied; computed with the BVNET tool, DOY: day of year.

growth across the entire Camargue region was early in 2017, when compared to growth in 2016. This was due to more favorable weather conditions at the beginning of the crop cycle. These phenological parameters can be considered good indicators for rice monitoring and can be mapped over the studied region to analyze farmers' strategies.

The choice of cultivar (early or late) can be crucial for crop development. Research in genetic selection has developed various cultivars that better adapt to weather conditions, resist pathogens, and correspond to market expectations. Cultivars can be classified according to their precocity. Late varieties with a crop cycle greater than or equal to 100 days are defined as productive but may suffer from poor conditions at the end of the cycle in the late season, because of lower temperature and radiation. Early varieties, with a crop cycle of around 80 days, may allow a second sowing, or a shift in the cycle, and are recommended in organic agriculture or as a means of limiting inputs. A typology is added according to the grain size (see Table 4 in Supplementary Material 5). There are relationships between the grain size, its main constituents, and the quality. Camargue farmers have various strategies for choosing cultivars depending on the start of the season and market demands (Mouret and Leclerc 2018). Some of them prefer to select late varieties that are less sensitive to climatic hazards (to avoid low temperatures at the beginning of the cycle), while others prefer to mix early, medium, and late, deciding on the sowing date according to the temperatures and the advice given by the CFR (Centre Français du Riz; French Rice Center). Figure 5 shows a comparison of the mean values and the standard deviation of LAI profiles computed for all fields planted with the same cultivar for the two years studied (information from the surveyed farmers). These profiles are obtained using the first equation given in Supplementary Material 4, applied to all days of the year (x represents the time scale as DOY from 1 to 365; the various fitted parameters are described below the first equation in Supplementary Material 4). A significant shift (up to 20 days) in the LAI profiles was observed between early and late

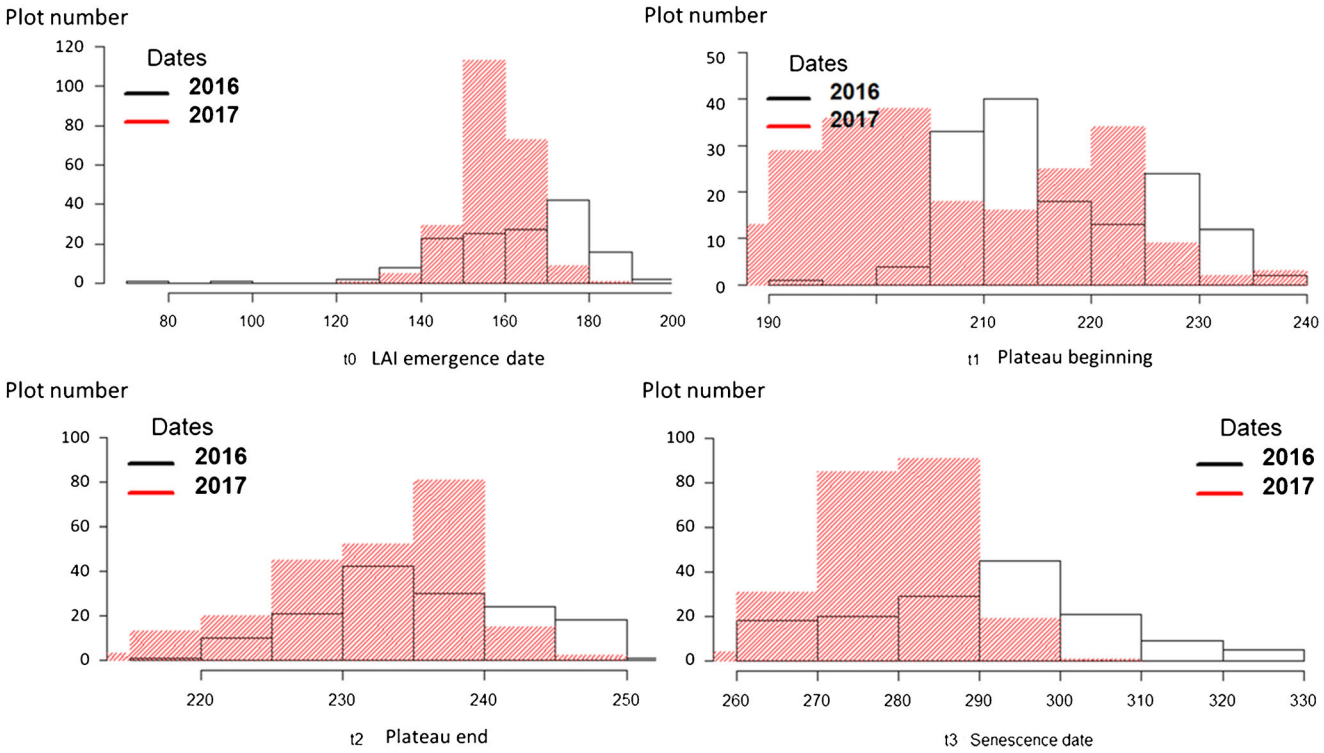


**Fig. 4** Distributions of phenological parameters extracted from the daily interpolations of LAI (leaf area index). See Supplementary Material 4 for the details on parameters computation. The x-axis corresponds to days of year (DOY).

cultivars, depending on the sowing date. The Volano cultivar (early variety) always appeared in advance of the later Gageron variety according to the LAI profiles, as expected. A large variability in the maximum values of LAI was also observed for the same cultivar. This can be explained by soil heterogeneities and the various technical practices found at the field scale.

A correlation analysis between yield data provided by the farmers and the cumulative LAI values for each phenological stage was done and have shown that the highest correlation values between LAI and yield were for the mature period

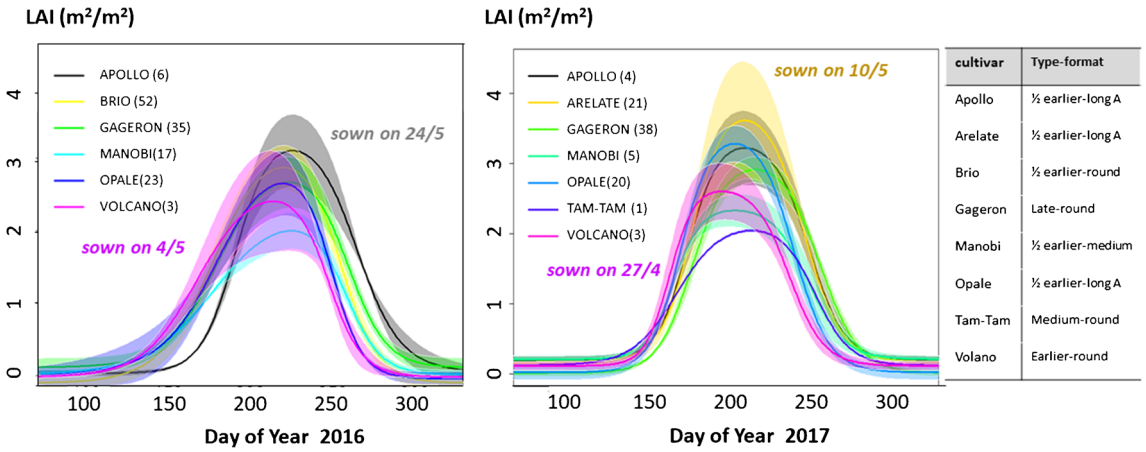


**Fig. 5** LAI (leaf area index) profiles computed from all rice fields planted with the same variety (information given by farm surveys). The envelope curve corresponds to the standard deviation, the middle line to the mean value; rice variety can be classified according to its earliness, its type, and its size or format (long A, B, or medium). The classification of the different varieties can be found on the CFR website (http://www.centrefrancaisduriz.fr/tableau_synthetique-47.html).

(between *t2*+23 days and *t2*+51 days, *t2* being the end of plateau, see Supplementary Material 4 for the details of the *t2* computation and Supplementary Material 7). The significant determination coefficients between LAI and yield for this stage were $R^2$= 0.58 in 2016 (RMSE=1.46) and $R^2$=0.73 in 2017, (RMSE=0.96) (these values were obtained using the Spearman method with *P*-value <0.01).

### 3.2 Analysis of STICS simulations

Simulations have been made for the different strategies for the two studied years. The results presented at both farm (shown in Supplementary Material 2) and Camargue levels in Table 2 correspond to the year 2016, chosen as a standard year with no exceptional weather events reported by the French weather service. The values obtained for 2017 are discussed in parallel in the text and compared to 2016 at the end of this section. The corresponding mean value of the yield simulated by the STICS crop model, considering constant inputs (strategy 0), was 5.74 t·ha$^{-1}$ in 2016 and 5.21 ton/ha in 2017. The first value was slightly higher for 2016 (+ 0.64 t·ha$^{-1}$) than the declarations made by the farmers for the IGP for the entire Camargue region (5.10 t·ha$^{-1}$). This first result must be considered with caution, since the simulation reproduced a study case corresponding to the mean values of our surveys. No comparison with IGP declarations was possible in 2017 because data were not available from CFR.

For strategy 1 case, remote sensing data was only used at the initial stage for mapping the land use, allowing rice to be distinguished from the other crops. The yields estimated over the entire Camargue area ranged between 4 and 9.10 t·ha$^{-1}$ in 2016 and between 2.20 and 8.20 t·ha$^{-1}$ for 2017. Globally, the simulations overestimated the yields for the two years (mean value 6.91 t·ha$^{-1}$ in 2016 and 6.10 t·ha$^{-1}$ in 2017), probably because of the systematic nitrogen applications. Values for actual yields provided by the farmers were lower due to various factors that the model does not yet take into consideration, such as some pests, diseases, and saline issues.

In the strategy 2 case, the introduction of the LAI variability as input in STICS significantly improved the yield estimation for the two years, compared to the previous strategy over the Camargue region. In 2016, the determination coefficient is higher 0.56 compared to 0.13 (Table 2). The bias was corrected, and the root mean square error was reduced to 1.29 t·ha$^{-1}$. At farm scale, the range of yield variation is the same as that at the regional level (Camargue area), between 3.10 and 5.71 t·ha$^{-1}$ with an RMSE of 1.26 t·ha$^{-1}$. However, the bias was higher. This farm was located in the south of Camargue, close to the sea, where the soils tend to be shallow. Some of the fields had salinity issues, resulting in lower yields (salinity is not simulated by the model).

Strategy 3 involved more information from remote sensing and used the sowing date computed for each field. At the farm scale, the results improved for $R^2$ and advanced from 0.24 to 0.53, but the bias increased. At the regional scale, the efficiency decreased from strategy 2 to 3. The introduction of SD did not seem to improve model performances. Surveys from the various farmers were heterogeneous, with certainly higher uncertainty on the sowing date; this could explain such results. A larger sample of farmers, and more accurate information, would be necessary to better understand the simulation uncertainties.

Strategy 4 based on an optimization method (simplex) to retrieve the initial soil nitrogen parameters using LAI observations produced the best results at the farm scale (Fig. 6b). The values of Nmin obtained after optimization varied from 0 to 120 kgN·ha$^{-1}$, and those for Norg were between 0.05 and 0.09% (Fig. 6a). These values were coherent and compared well to the few measurements available in this area (Ruget et al. 2016; Irfan 2013). The model performance of yield estimation at the farm scale showed an RMSE of 0.53 t·ha$^{-1}$. The fields that appeared the most scattered corresponded to fields with salinity issues. Fields with high salinity content are generally located in the southern part of the Camargue area, on deep soil, and at a topography sometimes below the sea level.

For the regional level, even if a significant increase of the determination coefficient is observed when remote sensing data are included in the simulations (strategies 2-3-4), the standard error still remained higher than at the farm level (*RMSE* = 1.59). At Camargue level, the lower score can be explained by the variabilities in observations given by farmers. As already mentioned, some farmers gave average values of yields for the same rice variety, others clustered several fields according to their water management, while others gave values for each rice field (this last case also explains why the results were higher at farm level than at regional level). In spite of this, the variation interval obtained at regional level gave relevant values compared to those given by the CFR.

Figure 7a shows an example of yield map obtained for the whole Camargue in 2016. The distribution of values for the two studied year is displayed below (Fig. 7b). The two years have globally similar distribution with majority of values between 5 and 6 t·ha$^{-1}$. Significant differences between the maps obtained for the two years are due to crop rotations. Wheat or sunflower have replaced rice fields for many farms (37% of the total of rice fields were changed). When rice is kept for two successive years (for more than 62% of fields), the highest yields were often observed at the same locations, this being certainly due to better soil nutrient status. Zooms can be done on specific areas such as the farm illustrated for the 2016 and 2017. The observed variations can be related to the soil type or technical practices (including cultivar variations). In the Southeastern Camargue, most of the time, the fields having the lowest yields were those having soil with a high salinity content. Numerous papers in the literature have confirmed that

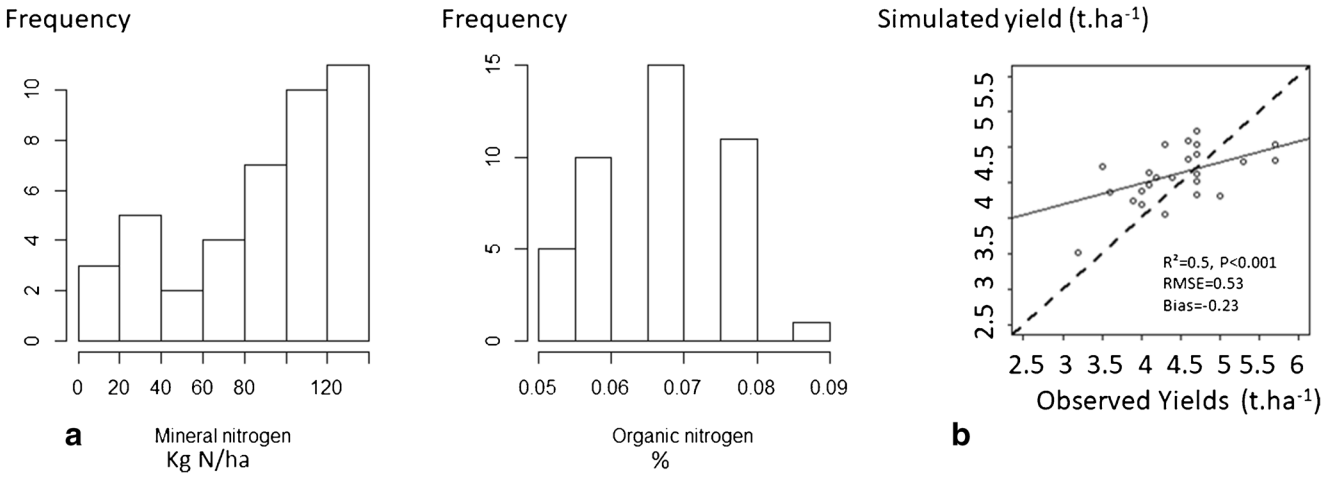


**Fig. 6** **a** Mineral and organic nitrogen values obtained after optimization using observed LAI (leaf area index) from Sentinel-2 (frequency corresponds to the number of simulated fields; **b** comparisons between observed and simulated yields (given in tons per hectare) for strategy 4 at the farm level (the simulated farm comprised 50 fields).

salinity has significant negative effects on rice yield without impacting LAI evolution (Gay et al. 2010; Fabre et al. 2005; Marcos et al. 2018). High salinity levels were often associated with reduced grain dimension and weight. Indeed, Radanielson et al. (2018a) and Radanielson et al. (2018b) noted an increase in the growth of some plant varieties in the presence of salt, but with less grain development. Therefore, it is possible for yield to be low even if LAI values are high. This phenomenon is explained by increased absorption of nutrients by the roots, due to the difference in osmotic potential between the plant and the soil solution.

No specific measurements were made to quantify soil salinity during our study period. We considered the qualitative information provided by the surveyed farmers who have a good level of knowledge about their fields. In the past, the farmers have measured salinity on some of their fields, and frequently the same fields have had the same issues. However, no statistical analysis can be performed from these past measurements because they were neither made at the same period nor with the same protocol. More investigations must be done in the future on this point to better consider this effect.

### 3.3 Discussion

These first simulations done with the STICS crop model and Sentinel-2 data on Camargue area have shown that Sentinel-2 data represent an important contribution for crop monitoring, as already noted by different authors (e.g., Veloso et al. 2017;

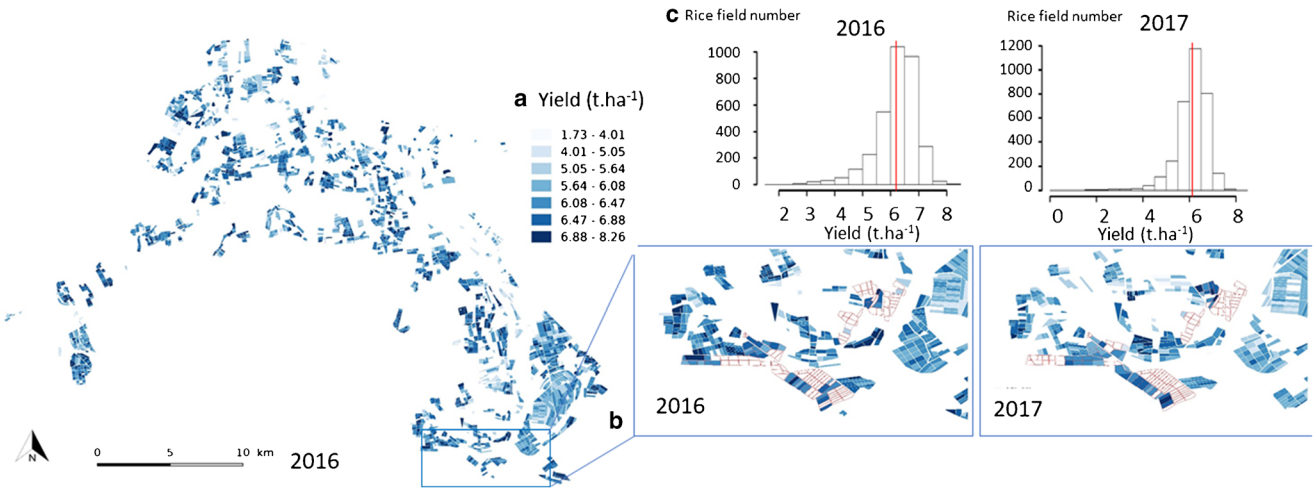


**Fig. 7** Production map simulated from STICS combined with Sentinel-2 data for 2016 at **a** Camargue and **b** farm scale (same colors for the different maps and the two years) with **c** the distribution of yield values obtained for the two studied years for the whole Camargue area (the vertical red line corresponds to the mean value).

Battude et al., 2016), but most of these last studies were more focused on cereals such as corn or wheat and not yet on rice. Up to now, there have been no accurate maps of yearly rice production for the entire Camargue region. The only available information comes from farmer declarations in the form of RPG maps (parcels registered each year to receive aid from the Common Agricultural Policy http://professionnels.ign.fr/rpg), which are only available the following year and do not represent all fields (due to variations in crop planning). These maps provide information on the area of rice cultivated but nothing on the technical practices, yield, or the quality of production in the fields.

The high spatial resolution of Sentinel-2 data represents a very useful information for crop monitoring through the analysis of LAI temporal profiles. Delmotte et al. (2011) noted that the Camargue rice agrosystems present a high yield variability due to various factors that are difficult to assess at the regional scale. The rice variety can be a criterion, among others, to categorize yield variability. Each year, the French Rice Center (CFR) provides reports of their experiments conducted across the Camargue area, where several cultivars are monitored on around 37 farms in Camargue area and characterized by various indicators, including yield (see http://www.centrefrancaisduriz.fr/publications-20.html). In 2016, for example, the highest yields were observed for the following varieties: Manobi, Gines, and Gageron. Opale and Mambo varieties presented the lowest yields. Sentinel-2 data can provide useful information on the varieties' precocity from the analysis of the temporal variation of LAI profiles for the whole territory of Camargue.

The combined use of the STICS crop model with LAI derived from Sentinel-2 data allowed the quantification of the crop development variability's impact on yield estimation. Various statistical analyses have been performed to evaluate the relationships between LAI and yield during different periods in the crop cycle. The highest determination coefficient (0.58 in 2016, RMSE = 1.46, 0.73 in 2017, RMSE =0.96) was found for LAI max (see Supplementary Material part 7, where a graph shows the relationship observed between LAI and observed yield).

In the standard version of STICS (without the use of remote sensing data), phenology was calibrated by adjusting the thermal time requirements (°C $day^{-1}$) between several factors: (i) emergence and maximum leaf area increase, (ii) beginning of stem elongation and maximum LAI, (iii) emergence and beginning of grain filling, (iv) flowering and maturity, and the leaf life duration (°C $day^{-1}$). Each parameter, depending on rice variety, is difficult to inform spatially. The introduction of Sentinel-2 LAI values as forcing inputs allowed to estimate yield values similar to those declared by the farmers in our surveys and in their reports for the IGP at regional level for strategy 2. However, some fields were always poorly estimated due to salinity problems, not considered by the model. Another source of error can be due to the presence of weeds in certain fields. Weeds have a strong negative impact on yield (Audebert et al. 2013; Delmotte et al. 2011), but not necessarily on LAI estimations. The majority of farms use chemical treatments (herbicides) to control weeds (only approximately 10% use organic management practices). According to the weed species (mainly *Echinochloa* and *Cyperaceae*) and the period of their apparition, it is often difficult to distinguish rice from other plants in temporal LAI profiles. However, we noticed in summer that the fields that appeared darker in the colored composite image (Fig. 8a) generally corresponded to fields with many weeds. The weeds appear to infiltrate fields from the boundaries and with time, gradually cover the entire field. We noticed that fields with *Cyperaceae* weeds usually presented higher values of the NDVI standard deviation, particularly in summer when these weeds are yellow and can be distinguished from the green rice plants (Fig. 8b). However, we did not have enough observations of weeds in the rice fields at the Camargue scale to be able to propose a weed contamination map. Deeper investigation of this issue should be conducted to develop an operational method based on a common spectral index such as NDVI which is easy to compute.

Pernollet et al. (2017) analyzed the impact on weed emergence from certain agricultural practices such as post-harvest stubble management, rice density, and soil preparation before sowing. They found that rice density significantly impacts weed emergence. Niang et al. (2016) analyzed six scenarios for the rice intercrop period, affirming that post-harvest flooding of rice fields facilitates straw and weed seed decomposition and is more economical. Delmotte et al. (2011) reported that the yield gap due to weeds ranged from 2.8 to 7.8 t·$ha^{-1}$ depending on other environmental factors. Fogliatto et al. (2010) and Vidotto et al. (2007) suggest that weeds are the worst noxious organism for rice crops and estimated that without weed control, 90% of yield could be lost. Our first observations show that during some periods (mainly in summer), and for some species (*Cyperaceae*), analysis of the temporal and spatial variability of NDVI at the field scale can enable the identification of certain weed-invaded fields. For future simulations, we can imagine weighting the yields by considering the contaminated surfaces. This will be the next step following the current study.

Sometimes yield values underestimated by the STICS model can be explained by the field's crop history (i.e., the previous crops during the months before rice implantation). For example, some farmers plant green manure such as alfalfa or ray grass and open the fields for grazing by cattle. This generally implies higher nitrogen content in the soil, which leads to better conditions for rice growth. We did not consider the field history in the various simulation strategies (except for strategy 4 through the estimation of Norg). The fields whose yields were underestimated by STICS for simulations without

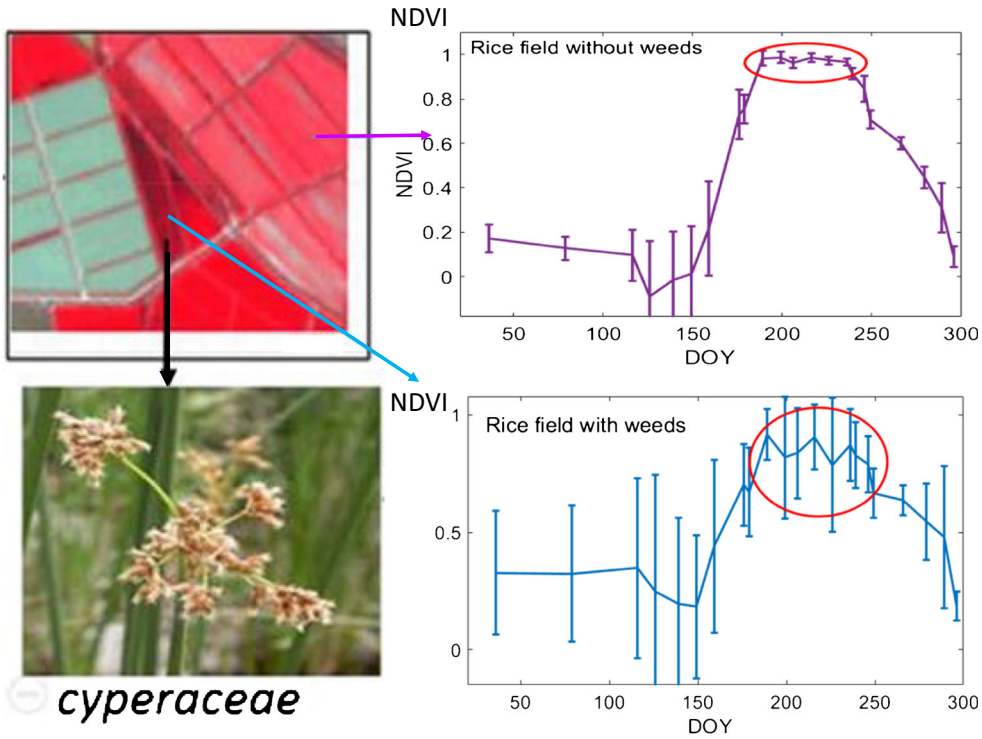


**Fig. 8** Colored composite (in red, band 8; in green, band 4; in blue, band 3) of Sentinel-2 image acquired on July 11, 2016, over rice fields. The dark color indicates weed presence (*Cyperaceae* species). Mean values of *NDVI* (normalized difference of vegetation index) computed for two rice fields, the standard deviation of *NDVI* was higher for the field with weeds.

optimization (in Fig. 7) were the fields on which the previous crop was either soybean or sunflower. These two crops have a beneficial effect on the following crop rotation. As a legume, soybean helps to fix nitrogen and leaves a nitrogen residue that is reusable by the next crop, and sunflower enables improved rooting (which has a role in soil structuring) and a rise in mineral components (oral communication from P. Debaeke, INRA Toulouse).

Jin et al. (2018) have discussed the different sources of errors in crop modeling combined with remote sensing data and concluded that the trend is to use different models to obtain an estimation of errors. Li et al. (2015) have tested the hypothesis that an ensemble of models reduces uncertainty. Indeed, the assessment of rice yield is not easy and can be quite complex, since many factors are involved, and uncertainties appear at different levels. Accuracy of weather and soil data can also affect the accuracy of the yield model. All factors cannot be assessed from remote sensing, but some related to the phenology and certain agricultural practices are now more accessible with clear optical images, as shown with, e.g., sowing date in our study. If clouds are frequent on specific areas, microwave data can possibly complete the database. Indeed, radar and optical data can be complementary to each other because they offer different perspectives of agroecosystems, providing different information according to their specificity (Nasrallah et al. 2019; Bouvet and Thuy Le 2011; Ndikumana et al. 2018a). Both types of data can be merged and provide useful information for decision-making and the analysis of various scenarios related to global change (Zhou et al. 2019).

## 4 Conclusion

This study aimed to evaluate the contribution of Sentinel-2 data for monitoring the phenological rice calendar in the Mediterranean climate and to assess the spatial variability of production. The high frequency of the revisit time of Sentinel-2 (A and B) satellites over the same area made it possible to obtain many cloudless images of the Camargue region and to apply a phenological model assessing the main stages of rice growth. It is the first time that temporal profiles of LAI obtained from Sentinel-2 data with the BVNET tool are analyzed for all the rice plots in the Camargue region. Analysis of the distributions of some key phenological parameters describing the rice cycle, derived from the PHENOTB tool, allowed to characterize spatial variability of agricultural choices. This study has shown that these tools and these new free data acquired at fine resolution are well suitable for rice monitoring and operational to be applied in various environmental contexts. The derived LAI maps have shown great spatial variability at both farm and Camargue levels. Earlier and later rice varieties with different sowing dates could be distinguished. The introduction of such data in a crop model allowed to assess to the spatial

variability of the rice production for the whole studied area and improved the estimations, particularly using a strategy with optimization of initial nitrogen values in the soil.

This proposed method based on the combined use of these recent remote sensing data acquired at high resolution with a crop model is a promising method to improve rice yield estimation and assess the spatial variability of agricultural practices performed at the regional level. All the data, tools, and models used in this study are in free access. This method can be reproducible in other regions where rice plays an important economic and environmental role. The availability of cost-free data provided by the THEIA pole is an advantage for operational applications. The fusion of multispectral data acquired in visible and radar ranges should also provide more accuracy in the future, without the constraints due to weather variations. This spatial information should play an increasingly important role in the development of useful tools for sustainable agriculture.

### Glossary

BVNET: Biophysical variables, neural network (tool developed at INRAE EMMAH to estimate biophysical variables such as LAI)

Can-eye: Software to estimate LAI from hemispherical photographs developed by INRAE EMMAH https://www6.paca.inrae.fr/can-eye

CFR: Centre Français du Riz, French Rice Center

DSSAT: Decision Support System for Agrotechnology Transfer

ESA: European Space Agency

IGN: French National Geographic Institute

IGP: Indication Géographique Protégée, label indicating production from a specific geographical area

LAI: Leaf area index

MAJA MACCS ATCOR Joint Algorithm: is a processor for cloud detection and atmospheric correction developed by CNES-CESBIO teams in Toulouse, France

PhenOTB Orfeo: toolbox to estimate phenology parameters

RF: Random forest method

RPG: Registre Parcellaire Graphique, corresponds to the plots declared by the farmer each year in order to receive state subsidies

STICS: Simulateur mulTI-disciplinaire pour les Cultures Standard, or multidisciplinary simulator for standard crops

SVM: Support vector machine (classification method)

THEIA: French Data Center, platform delivering remote sensing products, https://www.theia-land.fr/pole-theia-2/

Valeri: Validation of Land European Remote sensing Instrument

**Supplementary Information** The online version contains supplementary material available at https://doi.org/10.1007/s13593-021-00697-w.

**Acknowledgements** The authors thank the farmers, who kindly answered all of the surveys, and Margot Ribaud and Santiago Kennedy, the students who participated in this work. We thank Ben Boswell for English reviewing.

**Authors' Contributions** Conceptualization and methodology: DC, LH, VD, HD, KI, NB, FF, and FR. Investigation: DC, LH, HD, KI, and FF. Writing—original draft preparation: DC. Writing—review and editing: LH and KU. Funding acquisition: DC, NB, and LH.

**Funding** A part of this study was funded by the French National Center of Spatial Studies (CNES with a TOSCA project).

**Data Availability** The datasets generated during the current study are available from the corresponding author on reasonable request. Supplementary material provides the main equations and parameterizations.

## Declarations

**Ethics Approval and Consent to Prticipate** Informed consent was obtained from all individual participants included in the study.

**Conflict of Interest** The authors declare no competing interests.

## References

Audebert A, Mouret JC, Roques S, Carrara A, Hammond R, Gaungoo A, Sanusan S, Marnotte P (2013) Colonization and infestation ability of Bolboschoenus maritimus Palla in rice paddies of the Camargue, France. Weed Biol Manag 13(2):70–78

Baret F, Hagolle O, Geiger B et al (2007) LAI, fAPAR and fCover CYCLOPES global products derived from VEGETATION - Part 1:, principles of the algorithm. Remote Sens Environ 110(3):275–286. https://doi.org/10.1016/j.rse.2007.02.018

Battude M, Al Bitar A, Brut A et al (2017) Modeling water needs and total irrigation depths of maize crop in the south west of France using high spatial and temporal resolution satellite imagery. Agric Water Manag 189:123–136. https://doi.org/10.1016/j.agwat.2017.04.018

Battude M, Bitar A, Morin D et al (2016) Estimating maize biomass and yield over large areas using high spatial and temporal resolution Sentinel-2 like remote sensing data. Remote Sens Environ 184:668–681. https://doi.org/10.1016/j.agwat.2017.04.018

Bazzi H, Baghdadi N, El Hajj M et al (2019) Mapping paddy rice using Sentinel-1 SAR time series in Camargue, France. Remote Sens 11:887. https://doi.org/10.3390/rs11070887

Boote KJ, Jones JW, Pickering NB (1996) Potential uses and limitations of crop models. 88(5):704–716

Boschetti M, Nelson A, Nutini F, Manfron G, Busetto L, Barbieri M, Laborte A, Raviz J, Holecz F, Mabalay M, Bacong A, Quilang E (2015) Rapid assessment of crop status: an application of MODIS and SAR data to rice areas in Leyte, Philippines affected by Typhoon Haiyan. Remote Sens 7(6):6535–6557

Bouman BAM, van Laar HH (2006) Description and evaluation of the rice growth model ORYZA2000 under nitrogen-limited conditions. Agric Syst 87(3):249–273. https://doi.org/10.1016/j.agsy.2004.09.011

Bouvet A, Thuy Le T (2011) Use of ENVISAT/ASAR wide-swath data for timely rice fields mapping in the Mekong River Delta. Remote

Sens Environ 115(4):1090–1101. https://doi.org/10.1016/j.rse.2010.12.014
Bouvet A, Thuy Le T, Nguyen Lam D et al (2014) Estimation of agricultural and biophysical parameters of rice fields in Vietnam using x-band dual-polarization SAR. IEEE Int Symp Geoscience Remote Sens IGARSS 2014:1504–1507
Bregaglio S, Hossard L, Cappelli G, Resmond R, Bocchi S, Barbier JM, Ruget F, Delmotte S (2017) Identifying trends and associated uncertainties in potential rice production under climate change in Mediterranean areas. Agri Forest Meteor 237:219–232. https://doi.org/10.1016/j.agrformet.2017.02.015
Brisson N, Gary C, Justes E, Roche R, Mary B, Ripoche D, Zimmer D, Sierra J, Bertuzzi P, Burger P, Bussière F, Cabidoche YM, Cellier P, Debaeke P, Gaudillère JP, Hénault C, Maraux F, Seguin B, Sinoquet H (2003) An overview of the crop model STICS. Europ J Agro 18(3-4):309–332. https://doi.org/10.1016/S1161-0301(02)00110-7
Bsaibes A, Courault D, Baret F, Weiss M, Olioso A, Jacob F, Hagolle O, Marloie O, Bertrand N, Desfond V, Kzemipour F (2009) Albedo and LAI estimates from FORMOSAT-2 data for crop monitoring. Remote Sens Environ 113(4):716–729. https://doi.org/10.1016/j.rse.2008.11.014
Chakraborty M, Manjunath KR, Panigrahy S, Kundu N, Parihar JS (2005) Rice crop parameter retrieval using multi-temporal, multi-incidence angle Radarsat SAR data. Int J Photogram Remote Sens 59(5):310–322. https://doi.org/10.1016/j.isprsjprs.2005.05.001
Claverie M, Demarez V, Duchemin B, Hagolle O, Ducrot D, Marais-Sicre C, Dejoux JF, Huc M, Keravec P, Béziat P, Fieuzal R, Ceschia E, Dedieu G (2012) Maize and sunflower biomass estimation in southwest France using high spatial and temporal resolution remote sensing data. Remote Sens Environ 124:844–857. https://doi.org/10.1016/j.rse.2012.04.005
Clevers J, Vonder OW, Jongschaap REE et al (2002) Using SPOT data for calibrating a wheat growth model under Mediterranean conditions. Agron 22(6):687–694. https://doi.org/10.1051/agro:2002038
Confalonieri R, Acutis M, Bellocchi G, Donatelli M (2009a) Multi-metric evaluation of the models WARM, CropSyst, and WOFOST for rice. Ecol Model 220(11):1395–1410. https://doi.org/10.1016/j.ecolmodel.2009.02.017
Confalonieri R, Bellocchi G, Boschetti M, Acutis M (2009b) Evaluation of parameterization strategies for rice modelling. Span J Agric Res 7(3):680–686
Courault D, Hadria R, Ruget F, Olioso A, Duchemin B, Hagolle O, Dedieu G (2010) Combined use of FORMOSAT-2 images with a crop model for biomass and water monitoring of permanent grassland in Mediterranean region. Hydro Earth Syst Sciences 14(9):1731–1744. https://doi.org/10.5194/hess-14-1731-2010
Courault D, Demarez V, Guérif M, et al. (2016) Contribution of remote sensing for crop and water monitoring. Chap 4 in Land surface remote sensing in agriculture and forest. ISTE press Elsevier, edit Baghdadi et Zribi 113-177
Courault D, Hossard L, Flamain F et al. (2019) Assessment of agricultural practices from Sentinel 1 & 2 images applied on rice fields to get a farm typology in the Camargue region. in Proc Int Conf IGARSS IEEE; 28 July 2 August 2019 Yokohama, Japan, 4p
Courault D, Hossard L, Flamain F, Baghdadi N, Irfan K (2020) Assessment of agricultural practices from Sentinel 1 and 2 images applied on rice fields to develop a farm typology in the Camargue region. IEEE J Selec Topics Appl Earth Obs Remote Sens 13:5027–5035. https://doi.org/10.1109/JSTARS.2020.3018881
Delecolle R, Maas SJ, Guerif M et al (1992) Remote-sensing and crop production models - present trends. Int J Photogram Remote Sens 47:145–161
Delignette-Muller ML, Dutang C (2015) Fitdistrplus: an R package for fitting distributions. J Stat Softw 64:1–34
Delmotte S, Tittonell P, Mouret JC, Hammond R, Lopez-Ridaura S (2011) On farm assessment of rice yield variability and productivity gaps between organic and conventional cropping systems under Mediterranean climate. Eur J Agron 35(4):223–236. https://doi.org/10.1016/j.eja.2011.06.006
Demarez V (2018) Télédétection et fonctionnement hydrique des cultures à l'échelle du territoire. Mémoire HDR, Université Paul Sabatier Toulouse CESBIO 156p.
Fabre D, Siband P, Dingkuhn M (2005) Characterizing stress effects on rice grain development and filling using grain weight and size distribution. Field Crop Res 92(1):11–16. https://doi.org/10.1016/j.fcr.2004.07.024
Fogliatto S, Vidotto F, Ferrero A (2010) Effects of winter flooding on weedy rice (Oryza sativa L.). Crop Prot 29(11):1232–1240. https://doi.org/10.1016/j.cropro.2010.07.007
Fumoto T, Kobayashi K, Li C et al (2008) Revising a process-based biogeochemistry model (DNDC) to simulate methane emission from rice paddy fields under various residue management and fertilizer regimes. Glob Chang Biol 14(2):382–402. https://doi.org/10.1111/j.1365-2486.2007.01475.x
Gay F, Maraval I, Roques S, Gunata Z, Boulanger R, Audebert A, Mestres C (2010) Effect of salinity on yield and 2-acetyl-1-pyrroline content in the grains of three fragrant rice cultivars (Oryza sativa L.) in Camargue (France). Field Crop Res 117(1):154–160. https://doi.org/10.1016/j.fcr.2010.02.008
Gaydon DS, Probert ME, Buresh RJ, Meinke H, Suriadi A, Dobermann A, Bouman B, Timsina J (2012) Rice in cropping systems-modelling transitions between flooded and non-flooded soil environments. Eur J Agron 39:9–24
Gilardelli C, Stella T, Confalonieri R, Ranghetti L, Campos-Taberner M, García-Haro FJ, Boschetti M (2019) Downscaling rice yield simulation at sub-field scale using remotely sensed LAI data. Eur J Agron 103:108–116. https://doi.org/10.1016/j.eja.2018.12.003
Hansen JW, Jones JW (2000) Scaling-up crop models for climate variability applications. Agric Syst 65(1):43–72
Irfan K, (2013) Adaptation of the generic crop model STICS for rice (Oryza sativa I) using farm data in Camargue. PhD report, Thèse. Aix Marseille Université, 271 p.
Jarlan L, Boulet G (2014) Data assimilation for the monitoring of continental surfaces. Remote Sensing Imagery 283–319
Jin X, Kumar L, Li Z, Feng H, Xu X, Yang G, Wang J (2018) A review of data assimilation of remote sensing and crop models. Eur J Agron 92:141–152
Kennedy S (2018) Analyse des systèmes de cultures de riz en camargue et cartographie des principales pratiques culturales à l'aide d'images satellitaires Sentinel, Rapport Master 2 Université de Strasbourg, INRA EMMAH Avignon, 53p.
Launay M, Guerif M (2005) Assimilating remote sensing data into a crop model to improve predictive performance for spatial applications. Agric Ecosyst Environ 111(1-4):321–339. https://doi.org/10.1016/j.agee.2005.06.005
Li T, Hasegawa T, Yin X, Zhu Y, Boote K, Adam M, Bregaglio S, Buis S, Confalonieri R, Fumoto T, Gaydon D, Marcaida M III, Nakagawa H, Oriol P, Ruane AC, Ruget F, Singh B, Singh U, Tang L, Tao F, Wilkens P, Yoshida H, Zhang Z, Bouman B (2015) Uncertainties in predicting rice yield by current crop models under a wide range of climatic conditions. Glob Chang Biol 21(3):1328–1341
Longoni V (2010) Rice fields and waterbirds in the Mediterranean region and the Middle East. Waterbirds 33:83–96
Manfron G, Crema A, Boschetti M et al (2012) Testing automatic procedures to map rice area and detect phenological crop information exploiting time series analysis of remote sensed MODIS data. In: Neale CMU, Maltese A (eds) Remote Sensi Agric Ecosyst Hydro Xiv Proceed SPIE
Marcos M, Sharifi H, Grattan SR, Linquist BA (2018) Spatio-temporal salinity dynamics and yield response of rice in water-seeded rice fields. Agric Water Manag 195:37–46. https://doi.org/10.1016/j.agwat.2017.09.016

Merlin O, Duchemin B, Hagolle O, Jacob F, Coudert B, Chehbouni G, Dedieu G, Garatuza J, Kerr Y (2010) Disaggregation of MODIS surface temperature over an agricultural area using a time series of Formosat-2 images. Remote Sens Environ 114(11):2500–2512. https://doi.org/10.1016/j.rse.2010.05.025

Mosleh MK, Hassan QK, Chowdhury EH (2015) Application of remote sensors in mapping rice area and forecasting its production: a review. Sensors 15(1):769–791. https://doi.org/10.3390/s150100769

Mouret JC, Leclerc B (2018) Le riz et la Camargue: vers des agroécosystèmes durables. Educagri éditions ISSN:1768, 508 p–2274

Nasrallah A, Baghdadi N, El Hajj M et al (2019) Sentinel-1 data for winter wheat phenology monitoring and mapping. Remote Sens 11(19). https://doi.org/10.3390/rs11192228

Ndikumana E, Dinh Ho Tong M, Hai Thu Dang N et al (2018a) Estimation of rice height and biomass using multitemporal SAR Sentinel-1 for Camargue, Southern France. Remote Sens 10(9). https://doi.org/10.3390/rs10091394

Ndikumana E, Minh DHT, Baghdadi N et al. (2018b) Deep recurrent neural network for agricultural classification using multitemporal SAR Sentinel-1 for Camargue, France. https://doi.org/10.3390/rs10081217, 10

Nelder JA, Mead R (1965) A simplex method for function minimization. Comput J **7**:308–313

Niang A, Pernollet CA, Gauthier-Clerc M, Guillemain M (2016) A cost-benefit analysis of rice field winter flooding for conservation purposes in Camargue, Southern France. Agric Ecosyst Environ 231: 193–205. https://doi.org/10.1016/j.agee.2016.06.018

Palakuru M, Yarrakula K (2019) Study on paddy phenomics ecosystem and yield estimation using space-borne multi sensor remote sensing data. J Agrometeor 21(2):171–175

Paltasingh KR, Goyari P (2018) Statistical modeling of crop-weather relationship in India: a survey on evolutionary trend of methodologies. Asian J Agri Develop 15:43–60

Pazhanivelan S, Ragunath KP, Sudarmanian NH et al. (2019) Integrating time-series SAR data and ORYZA crop growth model in Rice area mapping and yield estimation for crop insurances. 42(3/W6)

Pernollet CA, Cavallo F, Simpson D, Gauthier-Clerc M, Guillemain M (2017) Seed density and waterfowl use of rice fields in Camargue, France. J Wildl Manag 81(1):96–111. https://doi.org/10.1002/jwmg.21167

Picazo-Tadeo AJ, Reig-Martínez E, Estruch V (2009) Farming efficiency and the survival of valuable agro-ecosystems: a case study of rice farming in European Mediterranean wetlands. Open Environmental Sciences 3:69–78

Radanielson AM, Cavallo F, Simpson D et al (2018a) Varietal improvement options for higher rice productivity in salt affected areas using crop modelling. Field Crop Res 229:27–36. https://doi.org/10.1016/j.fcr.2018.08.020

Radanielson AM, Gaydon DS, Li T, Angeles O, Roth CH (2018b) Modeling salinity effect on rice growth and grain yield with ORYZA v3 and APSIM-Oryza. Eur J Agron 100:44–55. https://doi.org/10.1016/j.eja.2018.01.015

Ruget F, Buis S, Irfan K et al. (2016) Parametrization of crop model using a regional agronomical database: rice in Camargue with STICS. *iCROPM 2016 International Crop Modelling Symp 2016-03-15-2016-03-17*) *Berlin* (*DEU*) 368-369 In : Crop Modelling for Agriculture and Food Security under Global Change 2016:437

Shen SH, Yang SB, Li BB, Tan BX, Li ZY, le Toan T (2009) A scheme for regional rice yield estimation using ENVISAT ASAR data. Sci China Ser D Earth Sci 52(8):1183–1194. https://doi.org/10.1007/s11430-009-0094-z

Shi WJ, Tao FL, Zhang Z et al (2013) A review on statistical models for identifying climate contributions to crop yields. J Geogr Sci 23:567–576

Singh U, Ritchie JT, Godwin D (1993) A user's guide to CERES Rice, V2. 10. International Fertilizer Development Center Muscle Shoals

Tang L, Zhu Y, Hannaway D, Meng Y, Liu L, Chen L, Cao W (2009) RiceGrow: a rice growth and productivity model. Njas-Wageningen J Life Sciences 57(1):83–92. https://doi.org/10.1016/j.njas.2009.12.003

Tao FL, Zhang Z (2013) Climate change, high-temperature stress, rice productivity, and water use in Eastern China: A New Superensemble-Based Probabilistic Projection. J Appl Meteorol Climatol 52(3):531–551. https://doi.org/10.1175/jamc-d-12-0100.1

Tornos L, Huesca M, Dominguez JA, Moyano MC, Cicuendez V, Recuero L, Palacios-Orueta A (2015) Assessment of MODIS spectral indices for determining rice paddy agricultural practices and hydroperiod. Int J Photogram Remote Sens 101:110–124. https://doi.org/10.1016/j.isprsjprs.2014.12.006

Tripathy R, Chaudhari KN, Mukherjee J, Ray SS, Patel NK, Panigrahy S, Parihar JS (2013) Forecasting wheat yield in Punjab state of India by combining crop simulation model WOFOST and remotely sensed inputs. Remote Sens Letters 4(1):19–28. https://doi.org/10.1080/2150704x.2012.683117

Trolard F, Bourrié G, Cary L et al (2018) Dynamiques biochimiques en rizières. Les apports du monitoring in situ. in Le riz et la Camargue: vers des agroécosystèmes durables. Educagri éditions, ISSN 1768-2274:193–205

Van Keulen H and Asseng SJCS., (2019). Simulation models as tools for crop management. 433-452.

Veloso A, Mermoz S, Bouvet A, le Toan T, Planells M, Dejoux JF, Ceschia E (2017) Understanding the temporal behavior of crops using Sentinel-1 and Sentinel-2-like data for agricultural applications. Remote Sens Environ 199:415–426. https://doi.org/10.1016/j.rse.2017.07.015

Vidotto F, Tesio F, Tabacchi M et al. (2007) Herbicide sensitivity of Echinochloa spp. accessions in Italian rice fields. Crop Protection, 26(3):285-293. https://doi.org/10.1016/j.cropro.2005.07.016

Yao FM, Tang YJ, Wang PJ, Zhang J (2015) Estimation of maize yield by using a process-based model and remote sensing data in the Northeast China Plain. Physics Chemis of the Earth 87-88:142–152. https://doi.org/10.1016/j.pce.2015.08.010

Yoshida H, Horie T (2010) A model for simulating plant N accumulation, growth and yield of diverse rice genotypes grown under different soil and climatic conditions. Field Crop Res 117(1):122–130. https://doi.org/10.1016/j.fcr.2010.02.007

Zhou G, Iu X, Liu M (2019) Assimilating remote sensing phenological information into the WOFOST model for rice growth simulation. 11(3):268. https://doi.org/10.3390/rs11030268